Does diphenylacetylene (tolan) fluoresce from its second excited singlet state? Semiempirical MO calculations and fluorescence quantum yield measurements

ARTICLE *in* CHEMINFORM · DECEMBER 1993

Impact Factor: 0.74 · DOI: 10.1021/j100153a008 · Source: OAI

3 AUTHORS, INCLUDING:

Camilla Ferrante
University of Padova
61 PUBLICATIONS **1,223** CITATIONS
SEE PROFILE

Bernhard Dick
Universität Regensburg
143 PUBLICATIONS **2,628** CITATIONS
SEE PROFILE

ARTICLES

Does Diphenylacetylene (Tolan) Fluoresce from Its Second Excited Singlet State? Semiempirical MO Calculations and Fluorescence Quantum Yield Measurements

Camilla Ferrante,† Uwe Kensy, and Bernhard Dick*

Institut für Physikalische und Theoretische Chemie, Universität Regensburg, 93053 Regensburg, Federal Republic of Germany

Received: July 12, 1993; In Final Form: September 28, 1993®

It is confirmed by measurements of fluorescence spectra and quantum yields that the fluorescence in tolan originates from the same state that causes the absorption band at lowest energy. The temperature dependence of the fluorescence quantum yield shows that this state is thermally deactivated with an activation energy of E_A = 14.0 kJ/mol. Geometry optimizations of the states S_0, S_1, and T_1 of tolan with the semiempirical AM1 method lead to planar structures with D_{2h} symmetry. Potential energy curves along the triple-bond stretching coordinate have been calculated for several low-lying excited states with a combination of the AM1 and the INDO/S methods. It is found that for large triple-bond lengths, the 1^1A_u-state with $\sigma\pi^*$ character becomes the lowest excited singlet state. It is proposed that thermal deactivation of $S_1(1^1B_{1u})$ leads to this state. Nonvertical excitation of 1^1A_u could explain the weak lines found in supersonic jet experiments below the onset of the $1^1A_g \rightarrow 1^1B_{1u}$ transition.

Introduction

Recently, the character and the energetic ordering of the low-lying electronic singlet states of diphenylacetylene (tolan) have been studied by high-resolution one- and two-photon spectroscopy in the supersonic jet[1] and inert gas matrices.[2] The ground state of tolan belongs to the point group D_{2h}. From the mutually exclusive selection rules observed in the one-photon and two-photon excitation spectra it was concluded that the point group is conserved in the lowest excited states. The longest-wavelength transition observed at 290 nm in solution is strong, long-axis-polarized[3] and hence can be assigned to a state of the irreducible representation $^1B_{1u}$. In the excitation spectra of the isolated molecule, weak lines were found below the electronic origin of the strong $1^1A_g \rightarrow 1^1B_{1u}$ transition. On the basis of an earlier π-electron calculation,[4] these lines were assigned to transitions to the states 2^1A_g and 1^1B_{2u}. In the condensed phase, no lines to the red of the $1^1A_g \rightarrow 1^1B_{1u}$ transition could be found.[2] In addition, semiempirical MO calculations including σ electrons strongly suggest that the state most likely responsible for the additional lines in the supersonic jet spectrum is 1^1A_u. The transition to this state of $\sigma\pi^*$ character is forbidden and should experience only a small red shift. Hence the question of the relative ordering of the singlet states in tolan seemed to be settled, with 1^1A_u being lowest in the isolated molecule and 1^1B_{1u} lowest in the condensed phase.

A recent paper by Hirata, Okada, Mataga, and Nomoto (in the following, abbreviated with HOMN) reported transient absorption measurements with picosecond time resolution following excitation of tolan into its longest-wavelength absorption band at 290 nm.[5] Three transient species X, Y, and T were assigned. From the rise and decay times, the excitation and relaxation sequence

$$S_0 \rightarrow X \rightarrow Y \rightarrow T \qquad (1)$$

was established. The species T was assigned to the triplet state due to its rather long lifetime which fell outside the range accessible with the picosecond apparatus. The decay time of X coincides with the rise time of Y and the fluorescence lifetime. Hence this species X was assigned to the fluorescing state. From the mirror symmetry of the absorption and fluorescence spectra it can be deduced that this is the same state (1^1B_{1u}) responsible for most of the absorption in the lowest energy absorption band of tolan.

The time-resolved measurements of HOMN showed that the decay from X to Y occurs within 8 ps at room temperature but is slowed down considerably at lower temperatures. An Arrhenius plot of $\ln \tilde{k}_X$, the observed rate constant, versus $1/T$ was performed to obtain an activation barrier of ≈8 kJ/mol for this process in several solvents with quite different viscosities. The decay of Y leading to T is temperature independent with a rate constant of $k_Y = 5 \times 10^9\ s^{-1}$. The absence of any viscosity effect on the decay of X → Y is taken as evidence against a conformational change involved in this process. (But only large-amplitude movements leading to twisted conformations were considered.) Hence, HOMN assign Y to the lowest excited singlet state of either B_{2u} or A_g symmetry, and consequently, the fluorescing state X had to be assigned to a higher singlet state. Fluorescence from higher excited singlet states is usually extremely weak in the condensed phase, and $S_2 \rightarrow S_0$ fluorescence with a quantum yield larger than 10^{-3} has been observed in few cases only. The best known example is azulene with an energy gap between S_1 and S_2 of 13 400 cm^{-1}.[6] For all other examples this energy gap is also large, e.g. ca. 8000 cm^{-1} in xanthiones[7] and ca. 14 000 cm^{-1} in naphthothiadiazines.[8] In tolan, however, transitions to states lower than 1^1B_{1u} are only seen in the supersonic jet, and the gap is less than 500 cm^{-1} in this case.

During the investigation of a photochemical reaction that leads to tolan as one of its products, we performed measurements of the fluorescence quantum yield Φ_F and MO calculations for this compound. Our investigation was triggered by an apparent discrepancy in the literature regarding Φ_F. One source[9] claimed that $\Phi_F \approx 0.0025$ at low temperature (probably 77 K), whereas the other[10] reported a value of $\Phi_F \approx 0.5$ almost independent of temperature. After we did our measurements, we learned about

† Present address: Department of Physical Chemistry, University of Padova, 2 Via Loredan, 35131 Padova, Italy.

• Abstract published in *Advance ACS Abstracts*, November 15, 1993.

0022-3654/93/2097-13457$04.00/0

the recent picosecond experiments.[5] We think that we can offer a satisfactory explanation of all experimental facts gathered so far for the condensed phase, and probably also for the isolated molecule. Our model does not involve any properties that are unusual for an aromatic molecule. In particular, we assign the fluorescent state X to 1^1B_{1u}, which is the lowest electronically excited state *at the equilibrium geometry of the electronic ground state*. However, another state with A_u symmetry not considered by HOMN is the lowest excited singlet state for greater lengths of the triple bond. This state is assigned to the transient species Y. The equilibrium bond lengths of the triple bond are calculated to be 1.200 Å in the ground state, 1.245 Å in the 1^1B_{1u} state, and 1.280 Å in the 1^1A_u state. Although these changes correspond to a considerable stretch of this strong bond, the overall movement is so small that a viscosity effect should not be expected.

Experimental and Calculational Procedures

Tolan (Aldrich) was purified by recrystallization from ethanol followed by vacuum sublimation (melting point 62 °C). Solvents diethyl ether, isopentane, and 3-methylpentane (3MP) from Merck (Uvasol spectrograde quality) were dried by chromatography on a column packed with Al_2O_3 (ICN Alumina B Super I) and silica gel (ICN Silica 100–200 aktiv 60A).[11] Samples in 3MP or in a diethyl ether–isopentane–ethanol mixture (volume ratio 5:2:5, EPA) with concentrations in the range (1–3) × 10^{-5} M were prepared in quartz cuvettes of 1 cm × 1 cm cross section and sealed after degassing by several freeze–pump–thaw cycles. In the course of this preparation 3MP was additionally dried by a K/Na alloy within the sealed glass apparatus. Fluorescence spectra were recorded with a Spex fluorolog consisting of two grating double monochromators (f = 80 cm), one for the excitation and one for the emission light beam, interfaced to a personal computer through home-built electronics. The sample was excited at 295 nm with a band-pass of 10 nm. Emission was detected at right angles with a 5-nm band-pass. The spectral response of this instrument was calibrated against a standard tungsten lamp (Optronic). The temperature in the sample chamber was measured with a Pt 100 resistance thermometer and varied by evaporation of liquid nitrogen. Absorption spectra were obtained in a Perkin Elmer 320 UV spectrometer equipped with a similar sample chamber.

Geometry optimizations for the electronic ground state of tolan and several excited singlet and triplet states were performed with the MOPAC program package.[12] The MNDO Hamiltonian[13] and the AM1 parameter set were used, and the PRECISE option was specified throughout. The AM1 method has been optimized for the reproduction of ground-state properties like enthalpies of formation, bond lengths, and bond angles.[14]

The MOPAC program package in the version available to us permits a limited amount of configuration interaction (CI) including excitations involving only a few orbitals. To get a more complete picture of the low-lying states, CI including singly and doubly excited configurations was performed with the CNDO/S method[15,16] augmented with the one-center exchange integrals of the INDO method.[17] This method yields vertical excitation energies to excited singlet and triplet states with comparative accuracy, and oscillator strengths for the transitions between states of the same multiplicity. In each calculation, 200 energy-selected configurations for singlet states and 300 for triplet states were included. The bonding properties of the correlated ground state and the excited states were evaluated by an all-valence-electron bond order[18] originally proposed by Cohen[19] as a generalization of the Coulson bond order for π-electron systems.

The MOPAC calculations were performed on an IBM-3090 mainframe computer (GWDG Göttingen), and for the INDO/S calculations, a personal computer (33 MHz i486 processor, 16 Mbyte storage) was used.

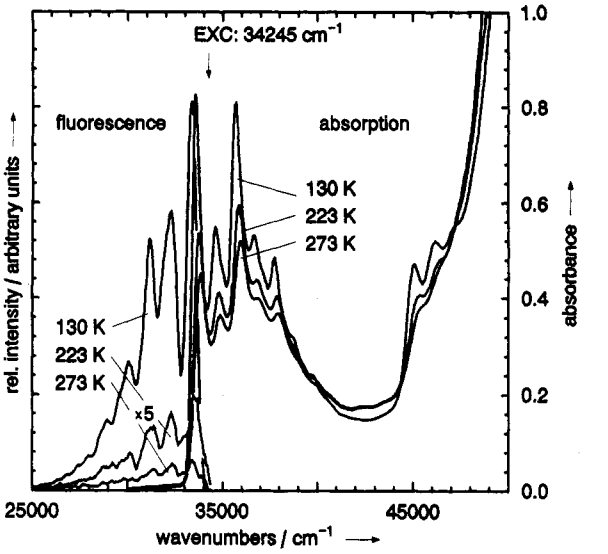

Figure 1. Absorption and corrected emission spectra of tolan in 3MP and EPA at various temperatures.

Results

Spectra and Quantum Yields. Fluorescence and absorption spectra of tolan in 3MP and EPA solvents for several temperatures are displayed in Figure 1. It is obvious that (i) the fluorescence quantum yield rises strongly with decreasing temperature, in contrast to the report in ref 10, (ii) the shape of the fluorescence spectrum is temperature independent, and (iii) the absorption spectrum is mirror symmetric to the fluorescence spectrum. Hence only one excited state fluoresces, and the same state is responsible for most of the intensity of the absorption band at ca. 290 nm. There exists a temperature-induced nonradiative deactivation channel for the fluorescing state. Integration of the absorption spectrum yields the oscillator strength according to

$$f = \frac{1}{n} 4.39 \times 10^{-9} \int \epsilon(\tilde{\nu})\, d\tilde{\nu} \qquad (2)$$

For the solvent 3MP (n_D = 1.3775) the value f = 0.81 is found. The relation between the Einstein B-coefficient and the transition dipole μ

$$B = \frac{2303c}{hnN_L} \int \frac{\epsilon(\tilde{\nu})}{\tilde{\nu}}\, d\tilde{\nu} = \frac{2\pi\mu^2}{3\hbar^2 n^2} \qquad (3)$$

yields $B = 6.27 \times 10^{19}$ cm^3 erg^{-1} s^{-2} and μ = 7.95 D (2.65×10^{-29} C m). The radiative rate constant k_r was calculated with Försters formula[20]

$$k_r^F = (2.88 \times 10^{-9}) n^2 \int \frac{\epsilon(\tilde{\nu})(2\tilde{\nu}_0 - \tilde{\nu})^3}{\tilde{\nu}}\, d\tilde{\nu} \qquad (4)$$

and with the Strickler–Berg relation[21]

$$k_r^{SB} = (2.88 \times 10^{-9}) n^2 \langle \tilde{\nu}_F^{-3} \rangle_{AV}^{-1} \int \frac{\epsilon(\tilde{\nu})}{\tilde{\nu}}\, d\tilde{\nu} \qquad (5)$$

$$\langle \tilde{\nu}_F^{-3} \rangle_{AV}^{-1} = \frac{\int I(\tilde{\nu}_F)\, d\tilde{\nu}_F}{\int \tilde{\nu}_F^{-3} I(\tilde{\nu}_F)\, d\tilde{\nu}_F} \qquad (6)$$

With the integration range 33 000 cm^{-1} < $\tilde{\nu}$ < 42 500 cm^{-1} and the center wavenumber $\tilde{\nu}_0$ = 33 750 cm^{-1} we find $k_r^F = 7.8 \times 10^8$ s^{-1}. With the same integration range for the absorption spectrum and the range 26 000 cm^{-1} < $\tilde{\nu}_F$ < 34 500 cm^{-1} for the fluorescence spectrum, the result of the Strickler–Berg relation is $k_r^{SB} = 6.3 \times 10^8$ s^{-1}.

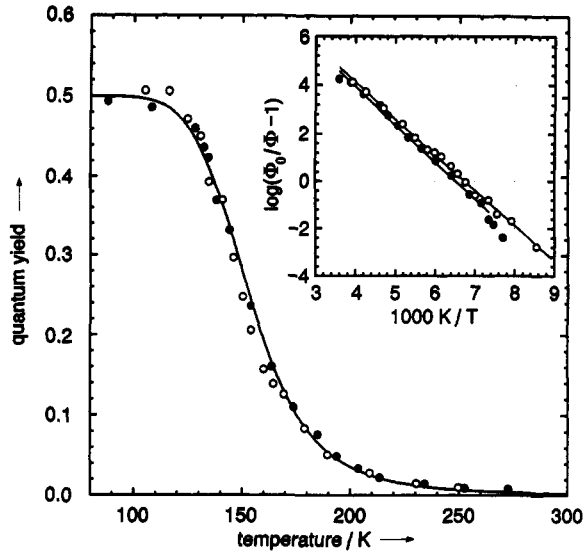

Figure 2. Absolute fluorescence quantum yield of tolan in EPA (full circles) and 3MP (open circles) as function of temperature. The full line is a fit of eq 8 to these data leading to an activation barrier of 14.0 kJ/mol. The inset shows the same data as a linearized Arrhenius plot, i.e. $\log(\Phi_0/\Phi - 1)$ vs $1/T$.

Absolute fluorescence quantum yields Φ_F were obtained from the integrated fluorescence spectra with quinine bisulfate in 1 N H_2SO_4 ($\Phi_F = 0.546$) as the standard.[22] This quantum yield is plotted as a function of temperature in Figure 2 for the solvents 3MP and EPA. From the quantum yield at room temperature ($\Phi_F(298\ K) = 3.36 \times 10^{-3}$ in 3MP) and the value for k_r from the Strickler–Berg relation, a lifetime of $\tau = 5.3$ ps is calculated in good agreement with the reported value of 8 ps.[5] This may be interpreted as an argument against a major contribution to the absorption spectrum from a second excited state.

A rate equation model that, in addition to the decay of the species X and Y to T or the ground state with rate constants k_X and k_Y, also considers forward and reverse reactions between the species with rate constants k_{XY} and k_{YX} yields the expression

$$\Phi_F = \frac{k_r(k_{YX} + k_Y)}{k_X(k_{YX} + k_Y) + k_{XY}k_Y} \tag{7}$$

for the fluorescence quantum yield from the species X. Here k_r is the radiative decay constant of X. An attempt to fit this expression to the experimental data with temperature-activated contributions in k_{XY} and k_{YX} resulted in $k_{YX} \ll k_Y$ in the whole temperature range. Hence a conclusion with respect to the barrier for the reverse reaction and the energetic ordering of X and Y cannot be drawn from the quantum yield data. That the reverse reaction is negligible can also be inferred from the fact that only monoexponential decay of the species X was observed in ref 5. If k_{YX} is neglected with respect to k_Y, the expression for the quantum yield (eq 7) becomes also independent of k_Y. The total decay rate $k_X + k_{XY}$ of the fluorescing state may be approximated by the sum of a temperature-independent part $k_0 = k_r + k_{nr}$ containing both fluorescence and a nonradiative contribution, and a temperature-activated term. The best fit of the corresponding expression for the fluorescence quantum yield

$$\Phi_F = \frac{k_r}{k_0 + k_a \exp(-E_A/RT)} \tag{8}$$

to the experimental data points is shown as the full line in Figure 2. The optimized parameters are $\Phi_F^0 = k_r/k_0 = 0.50$, $k_a/k_r = 1.15 \times 10^5$, and $E_A = 13.96$ kJ/mol. Taking again k_r from the Strickler–Berg relation, the frequency factor $k_a = 7.25 \times 10^{13}$ s^{-1} is obtained. This corresponds to a vibration with a wavenumber of 2420 cm^{-1}.

TABLE I: Heats of Formation (kJ/mol), Bond Lengths (Å), and Bond Angles (deg) Obtained from Geometry Optimizations with the AM1 Method[a]

	S_0	S_1	T_1
$\Delta H°_f$	409.83	798.70	623.64
	Lengths		
C1′–C1	1.2000	1.2367	1.2378
C1–C2	1.4059	1.3553	1.3525
C2–C3	1.4053	1.4342	1.4410
C3–C4	1.3928	1.3799	1.3705
C4–C5	1.3949	1.4016	1.4074
C3–H3	1.1000	1.1000	1.1004
C4–H4	1.1000	1.1011	1.1012
C5–H5	1.0998	1.0993	1.0978
	Angles		
C1–C2–C3	120.29	121.27	121.31
C2–C3–C4	120.05	120.73	120.72
C2–C3–H3	119.73	118.53	118.17
C3–C4–H4	119.74	119.99	120.27

[a] The electronic ground state S_0 was treated on the SCF level, and for the S_1 and T_1 states a limited configuration interaction was applied.

Calculations. Optimization of the geometry of the electronic ground state with a single determinant wave function and the AM1 Hamiltonian resulted in a planar structure having D_{2h} point group symmetry with a linear triple bond. The optimized geometry parameters and the heats of formation are given in Table I. A survey of the potential energy curve along the coordinate of phenyl ring torsion yielded a rather small barrier of only 0.9 kJ/mol located at the geometry with a perpendicular orientation of the phenyl groups. The experimental value for this shallow barrier is ≈2.5 kJ/mol,[1] which is also reproduced by elaborate ab initio calculations.[28]

Some attempts were made to optimize geometries of excited states. Since variation of all geometric parameters is very time consuming for an excited-state wave function, the constraint of planar phenyl groups was imposed. The center of symmetry was also retained, which is justified by the experimental observation of mutually exclusive selection rules for one-photon and two-photon transitions.[1,2] A twist of the phenyl group either in plane or out-of-plane as well as bending of the triple bond was admitted. Geometry optimization was performed with a limited configuration interaction wave function (MOPAC option CI = 4), taking into account the two highest occupied and two lowest empty orbitals from the closed-shell SCF calculation. The optimized geometries for the states S_1 (options SINGLET and ROOT = 2) and T_1 (options TRIPLET and ROOT = 1) were again planar and showed all symmetry elements of the point group D_{2h}. The geometrical parameters are collected in Table I. It is seen that the largest geometrical change with respect to the electronic ground state is a lengthening of the triple bond C1′–C1 and a considerable shortening of the bond C1–C2 to the phenyl substituent. Optimization of other roots for both multiplicities were only partly successful and revealed that several excited states are located in close vicinity. Hence the use of such a small configuration basis is questionable.

To gain better insight into the energetic ordering and spectroscopic properties of the low-lying excited states, an INDO/S calculation was performed at the AM1-optimized geometry of the electronic ground state. This calculation included 200 energy-selected singly and doubly excited configurations for the singlet states and 300 for the triplet states. Table II lists some of the results for the singlet states up to 50 000 cm^{-1} and the triplet states up to the energy of S_1. Three strongly allowed one-photon transitions are found in this region: two long-axis-polarized ($A_g \rightarrow B_{1u}$) and one polarized along the short in-plane axis ($A_g \rightarrow B_{2u}$). The oscillator strength ($f = 0.679$) and transition dipole ($\mu = 6.58$ D) for the lowest energy transition are in good agreement with the experimental values obtained for the first absorption band. The four lowest excited singlet states 1^1B_{1u}, 1^1B_{2u}, 1^1B_{3g},

TABLE II: Symmetries, Vertical Excitation Energies (in cm^{-1}), Oscillator Strengths f, Two-Photon Cross Sections δ (in Units of 10^{-50} cm^4 s^{-1}), and Two-Photon Polarization Parameters Ω of the Lowest Excited States of Tolan, Calculated with the INDO/S Method at the AM1-Optimized Ground-State Geometry, and the All-Valence-Electron Bond Orders Between Carbon Atoms for the Lowest States of each Multiplicity[a]

						Cohen bond orders				
	state	ΔE	f	δ	Ω	1'–1	1–2	2–3	3–4	4–5
S_0	$1\,^1A_g$	0				2.849	1.396	1.658	1.715	1.700
S_1	$1\,^1B_{1u}$	33 360	0.679			2.514	1.574	1.522	1.748	1.652
S_2	$1\,^1B_{2u}$	34 618	0.006			2.807	1.438	1.581	1.631	1.633
S_3	$1\,^1B_{3g}$	34 642		1.75	1.50	2.808	1.436	1.580	1.629	1.631
S_4	$1\,^1A_u$	34 779				2.145	1.601	1.595	1.723	1.693
S_5	$2\,^1A_g$	40 305		24.61	0.76					
S_6	$2\,^1A_u$	42 417								
S_7	$2\,^1B_{1u}$	44 528	0.067							
S_8	$3\,^1A_g$	45 350		147.19	0.76					
S_9	$1\,^1B_{2g}$	45 569		0.01	1.50					
S_{10}	$2\,^1B_{3g}$	47 567		0.74	1.50					
S_{11}	$2\,^1B_{2u}$	48 423	0.873							
S_{12}	$1\,^1B_{1g}$	48 923								
S_{13}	$3\,^1B_{1u}$	49 372	1.973							
T_1	$1\,^3B_{1u}$	21 020				2.611	1.566	1.513	1.748	1.624
T_2	$1\,^3A_g$	25 179				2.830	1.396	1.545	1.695	1.602
T_3	$1\,^3B_{2u}$	29 786				2.815	1.433	1.570	1.630	1.649
T_4	$1\,^3B_{3g}$	29 792				2.815	1.431	1.563	1.624	1.646
T_5	$2\,^3B_{1u}$	29 856								
T_6	$2\,^3A_g$	31 006								
T_7	$1\,^3A_u$	32 150								
T_8	$3\,^3B_{1u}$	34 262								

[a] For the atomic numbering scheme see Figure 3.

TABLE III: Configurational Composition of the Lowest Excited States of Tolan from the INDO/S Calculation[a]

state		configurations
$\|S_0\rangle$	=	$0.993\Phi_0$
$\|S_1\rangle$	=	$0.900\Phi_1^1 - 0.250\Phi_4^6 + 0.222\Phi_5^4$
$\|S_2\rangle$	=	$0.650\Phi_1^2 + 0.501\Phi_2^1 - 0.378\Phi_3^4 + 0.383\Phi_5^3$
$\|S_3\rangle$	=	$0.652\Phi_1^3 - 0.496\Phi_3^1 + 0.377\Phi_2^4 + 0.386\Phi_5^2$
$\|S_4\rangle$	=	$0.860\Phi_4^{13} + 0.265\Phi_4^{13} + 0.389\Phi_4^8$
$\|T_1\rangle$	=	$0.861\Phi_1^1 - 0.208\Phi_2^2 + 0.209\Phi_3^3 + 0.340\Phi_5^4$
$\|T_2\rangle$	=	$0.624\Phi_1^4 + 0.511\Phi_5^1 - 0.380\Phi_2^3 + 0.380\Phi_3^2$
$\|T_3\rangle$	=	$0.705\Phi_1^2 - 0.412\Phi_2^1 + 0.308\Phi_3^4 + 0.448\Phi_5^3$
$\|T_4\rangle$	=	$0.704\Phi_1^3 + 0.413\Phi_3^1 - 0.308\Phi_2^4 + 0.448\Phi_5^2$
$\|T_5\rangle$	=	$0.282\Phi_1^1 + 0.657\Phi_2^2 - 0.656\Phi_3^3$

[a] The configuration Φ_k^l denotes excitation of an electron from orbital ψ_k to the orbital $\tilde{\psi}_l$. Only configurations with coefficients $|c| > 0.2$ are listed. For the numbering of orbitals see text and Figure 3.

and $1\,^1A_u$ are found very close together. Their relative ordering might be different in the real molecule. Therefore, all four states have to be considered in the explanation of the photophysical properties. This ambiguity does not exist for the triplet states, where T_1 ($1\,^3B_{1u}$) and T_2 ($1\,^3A_g$) are well separated from the higher triplets and from each other.

An analysis of the configurations contributing more than 4% to the norm of the lowest five singlet and triplet states is shown in Table III. We label the occupied orbitals ψ_k of the ground state in descending order beginning with the highest occupied molecular orbital (HOMO). The virtual orbitals $\tilde{\psi}_l$ are numbered in increasing order beginning with $l = 1$ for the lowest unoccupied molecular orbital (LUMO). The promotion of an electron from ψ_k to $\tilde{\psi}_l$ leads to the singly excited configuration Φ_k^l, i.e. Φ_1^1 is the HOMO–LUMO transition. For completeness the closed shell reference configuration for the CI is denoted Φ_0. From Table III it can be seen that even the leading configurations of these lowest states involve five occupied and six unoccupied orbitals. The energy level diagram and the LCAO coefficient patterns of these most important orbitals are drawn in Figure 3. Three of these orbitals, namely $\psi_4(b_{2u})$, $\tilde{\psi}_5(b_{1u}7)$, and $\tilde{\psi}_6(b_{3g})$ have σ character with respect to the molecular plane, i.e. the 2s- and $2p_y$-orbitals of the carbon atoms are involved. The other MOs are π-orbitals consisting of carbon $2p_x$-orbitals only. The orbitals $\psi_2(a_u)$ and $\psi_3(b_{1g})$ as well as the empty orbitals $\tilde{\psi}_2(b_{1g})$ and $\tilde{\psi}_3(a_u)$ have vanishing coefficients at the two central carbon atoms. The excitations Φ_2^2, Φ_2^3, Φ_3^2, and Φ_3^3 can hence be considered as localized or charge-exchange configurations involving only the phenyl rings. Of the low-lying states, only T_5 has a leading contribution from these excitations. We may consider acetylene as the parent compound of tolan, which has two pairs of degenerate π-orbitals. Adopting the same axis convention as for tolan, these are the bonding orbitals π_x,π_y and the antibonding orbitals π_x^*, π_y^*. The orbitals π_y and π_y^* are almost completely conserved in the tolan orbitals ψ_4 and $\tilde{\psi}_6$. Although these orbitals have now σ-symmetry in the strict sense of the $\sigma - \pi$ separation theorem for planar molecules, they are energetically equivalent to π-orbitals and have to be considered for the low-energy excitations. Excitations involving one of these two orbitals and a π-orbital should hence display behavior typical for $n\pi^*$ or πn^* transitions. This relates in particular to the expected large spin–orbit coupling. The other two π-orbitals of acetylene mix strongly with the π-orbitals of the phenyl groups. Thus these two orbitals contribute only ca. 25% to the norm of the HOMO and the LUMO.

For the five lowest singlet states and the four lowest triplets a population analysis in terms of Cohen's all-valence-electron bond-order $B(I–J)$ has been performed. The results for the C–C bonds are listed in Table III. The greatest changes ΔB occur for the central bond C1'–C1 and the bond to the phenyl ring, C1–C2. Excitation from S_0 to S_1 leads to $\Delta B(1'–1) = -0.335$ and $\Delta B(1–2) = 0.178$. For excitation to T_1, the corresponding values are $\Delta B(1'–1) = -0.238$ and $\Delta B(1–2) = 0.170$. This is in good agreement with the lengthening of the central bond and shortening of the C1–C2 bond observed in the AM1 geometry optimizations of these states. This can be rationalized by the fact that the HOMO–LUMO excitation is the leading term in these two states. The HOMO is bonding with respect to the central bond and antibonding with respect to the bond to the phenyl group. For the LUMO the opposite is true. Since, however, both orbitals are delocalized, the change of the bond order produced by this excitation is smaller than unity.

For the states $1\,^1B_{2u}$, $1\,^1B_{3g}$, $1\,^3A_g$, $1\,^3B_{2u}$, and $1\,^3B_{3g}$ only small changes of the bond orders are found. This can be understood by considering that the empty orbital $\tilde{\psi}_4$ has a node structure

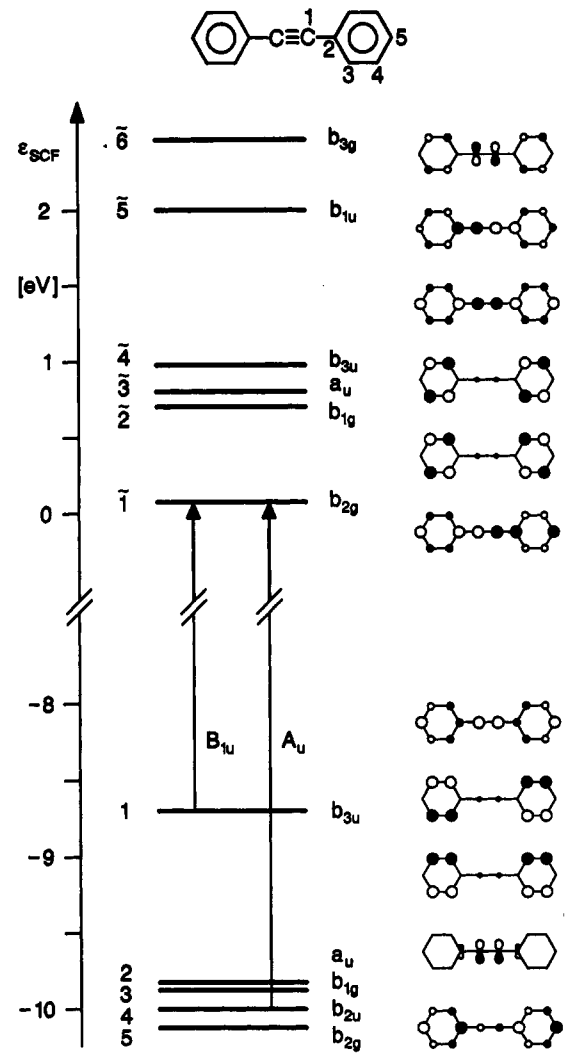

Figure 3. Energy level diagram and MO coefficients for the molecular orbitals involved in the low-lying electronic states of tolan obtained by the INDO/S method. Occupied orbitals are numbered in descending order, virtual orbitals in ascending order. The size of the circles corresponds to the coefficient of the atomic p_x-orbital for the particular MO, with full circles indicating positive sign. Note that the occupied orbital 4 and the virtual orbitals $\tilde{5}$ and $\tilde{6}$ have σ-symmetry with respect to the molecular plane. In this case the MO coefficients refer to the s and p_y atomic orbitals.

similar to that of the HOMO with respect to the two bonds of interest. Hence the excitation Φ_1^4 is fairly neutral with respect to these bond orders, as are the excitations involving only phenyl-localized orbitals mentioned above. This explains why almost no change of bond order occurs for the state T_2. For the states S_2 and S_3 as well as their triplet counterparts T_3 and T_4, a similar effect is produced by the cancellation of the opposite effects that the excitations Φ_n^1 and Φ_n^4 with $n = 2$ or $n = 3$ have on the bond orders.

Large changes $\Delta B(1'-1) = -0.704$ and $\Delta B(1-2) = 0.205$ are again found for the S_4 (1^1A_u) state. Its leading configuration is Φ_4^1. Since ψ_4 is almost entirely a two-center binding orbital, originating from the π_y of acetylene, removing an electron from it should contribute $\Delta B(1'-1) \approx -0.5$. The change is even greater since the LUMO is also antibonding for the same pair of atoms. Bond order changes of this size are rather rare for aromatic hydrocarbons. The largest values that we have encountered so far in similar INDO/S calculations were $\Delta B = 0.299$ and $\Delta B = -0.260$ for the bonds in the four-membered ring of biphenylene[23] in its S_1 state and $\Delta B = 0.302$ for the central bond in azulene also in its S_1 state. In both cases these excited states have unusually short lifetimes for this class of compounds, namely $\tau \approx 250$ ps for biphenylene[24] and $\tau \approx 2$ ps for azulene.[25] Hence, it is likely that the 1^1A_u state of tolan also decays very rapidly via internal conversion (IC). Due to its $\sigma\pi^*$ character and the resulting large spin–orbit coupling, intersystem crossing (ISC) to the triplet manifold should be an additional fast decay channel.

The strong decrease in the bond order for the central CC bond of tolan in the 1^1A_u state suggests that this state in its equilibrium geometry has a significantly longer central bond and a much lower energy. Since at the ground-state geometry the 1^1A_u state is only about 1250 cm^{-1} above S_1, it might well be the lowest excited state at its own equilibrium geometry. Thus it seems very likely that the coordinate relevant for the internal conversion between the two excited singlet states apparently involved in the excited-state dynamics is not the phenyl ring torsion or a bending mode of the central chain of the molecule but the stretching mode of the triple bond.

To explore the potential surfaces of the low-lying electronic states along this coordinate, we combined the enthalpy of formation from the AM1 method with the excitation energies obtained with the INDO/S method. Although two slightly different model Hamiltonians are used, this mixed approach offers several advantages. The AM1 method in the implementation available to us permits only the consideration of 100 Slater determinants generated from a maximum of five molecular orbitals. Hence, not even half of the most important orbitals could be included, and only a single configurational basis for all multiplicities can be constructed. In contrast, the INDO/S program generates spin-adapted configurations from all orbitals and selects those with the lowest energies, allowing for separate CI calculations with a large basis for each multiplicity. Further, its parameters have been chosen to yield good results for excitation energies, whereas the AM1 method was parametrized to reproduce ground-state properties. On the other hand, the INDO/S method is not useful for potential surfaces since the core–core interaction needs to be carefully balanced for this purpose. For a given geometry, the core–core interaction is the same in all electronic states, and an improper treatment of this contribution leads to a constant error for all states. In order to connect the energies from both methods, we assume that the ground-state SCF energy is correctly calculated with the AM1 method. Then the error in the total INDO/S energies for all states at a fixed geometry is given by the difference $E_{INDO}^{SCF}(S_0) - E_{AM1}^{SCF}(S_0)$ of the ground-state SCF energies between the INDO/S and the AM1 methods. The corrected energy $E(X)$ of a particular state X is calculated according to

$$E(X) = E_{AM1}^{SCF}(S_0) - E_{INDO}^{SCF}(S_0) + E_{INDO}^{CI}(X) \qquad (9)$$

Calculations were performed in the range $1.11\ \text{Å} \le R \le 1.33\ \text{Å}$ for the length of the triple bond with a stepsize of 0.005 Å. All other parameters were fixed at the equilibrium values of the electronic ground state (see Table I). The potential energy curves obtained in this way for the electronic ground state 1^1A_g, the four lowest excited singlet states (1^1B_{1u}, 1^1B_{2u}, 1^1B_{3g}, 1^1A_u), and the two lowest triplet states (1^3B_{1u}, 1^3A_g) are shown in Figure 4. The states 1^1A_g, 1^1B_{2u}, 1^1B_{3g}, and 1^3A_g all have an equilibrium distance of $R \approx 1.200$ Å. Their potential curves move almost parallel, i.e. the energy differences between these states are not affected by R. This is in line with the observation made above that these states involve mainly configurations which do not alter the electron density or the bond order in the triple bond.

The states 1^1B_{1u} and 1^3B_{1u} resulting from the HOMO–LUMO transition have their equilibrium at $R = 1.235$ Å and $R = 1.245$ Å, respectively. These bond lengths are in good agreement with those found by optimizing the geometry for a limited CI wave function and the AM1 Hamiltonian (see Table I). Hence a strong progression in the stretching vibration of the triple bond is expected for the optical absorption transition $1^1A_g \rightarrow 1^1B_{1u}$ and the corresponding fluorescence transition $1^1A_g \leftarrow 1^1B_{1u}$. As was already shown in Table II, this transition is the only one with

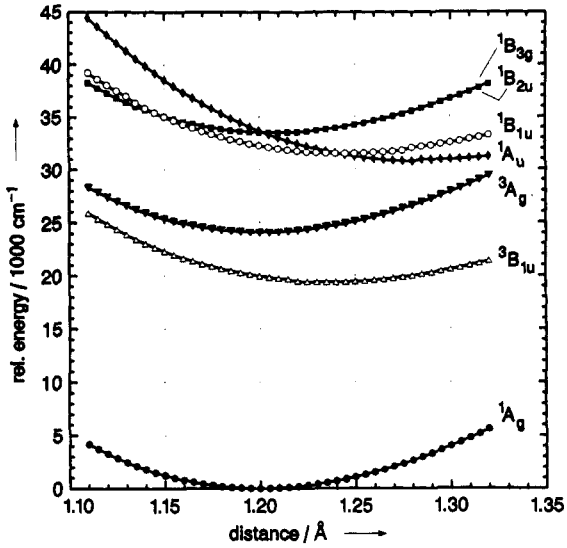

Figure 4. Potential energy curves for the lowest singlet and triplet states of tolan as a function of the length of the central CC triple bond. The electronic excitation energies with respect to the SCF ground state from an INDO/S calculation with singly and doubly excited configurations (200 singlets and 300 triplets) were added to the SCF potential energy curve of the closed shell ground state obtained from the AM1 method.

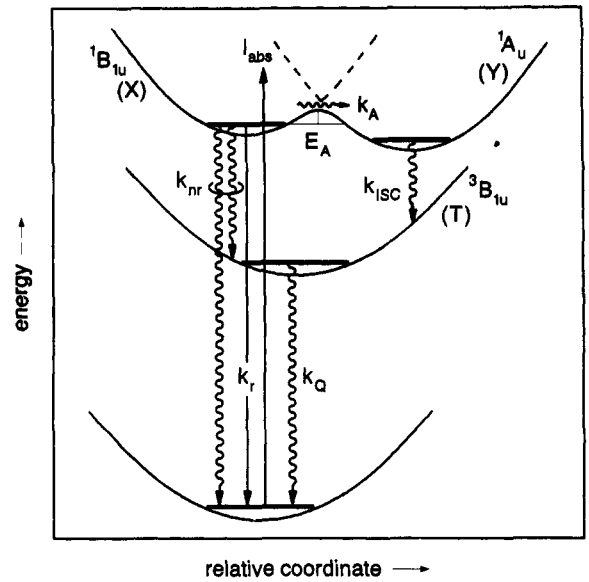

Figure 5. Schematic diagram of the potential energy curves and the kinetic model used to analyze the excited states dynamics in tolan. The initially excited state $^1B_{1u}$ decays radiatively back to the ground state 1^1A_g with rate constant k_r. A radiationless and temperature-independent decay leads with the total rate constant k_{nr} and unknown branching ratio to the states ^1A_g and $^3B_{1u}$. The decay to ^1A_u is thermally activated with activation energy E_A and frequency factor k_a. The state ^1A_u decays with rate constant k_{ISC} to the triplet state $^3B_{1u}$ which returns to the ground state with rate constant k_Q.

reasonable intensity to explain the longest-wavelength absorption band of tolan.

If the 1^1A_u state were neglected, as is the case in purely π-electron calculations, no crossing of any low-lying electronic states would occur. Due to the much weaker strength of the central C–C bond in this state, however, its potential curve crosses that of 1^1B_{1u}, 1^1B_{2u}, and 1^1B_{3g} to become the lowest excited singlet state at the equilibrium bond length of 1.28 Å. This length is closer to a standard double bond than to a triple bond.

Discussion

On the basis of the calculations presented above, we propose a model that in our opinion explains all experimental observations made so far for tolan without resorting to any unusual assumption. This model is schematically represented in Figure 5. The species named X and Y in the recent picosecond experiments[5] are assigned to the excited singlet states 1^1B_{1u} and 1^1A_u, and the relaxation X → Y involves the triple-bond stretching coordinate. The crossing point between these two potential curves leads to the activation energy of $E_A = 14$ kJ/mol derived from the temperature dependence of the fluorescence quantum yield. The preexponential factor $k_a = 7.2 \times 10^{13}$ s^{-1} found for this process agrees well with the frequency of $\nu = 6.7 \times 10^{13}$ s^{-1} (Raman line at 2220 cm^{-1} [26]) for the triple-bond stretching vibration. Gutmann et al.[2] have observed the vibrationally resolved spectrum of the $S_0 \rightarrow 1^1B_{1u}$ transition of tolan isolated in rare-gas matrices. They noticed a sudden increase of vibronic line widths ca. 1300 cm^{-1} above the origin. This indicates the presence of a fast decay channel at an excess energy of ca. 15 kJ/mol.

The reversal of the state ordering is brought about by a small relative movement of the central carbon atoms of less than 0.08 Å. The bond orders for the bonds to the phenyl rings are larger in these states than in the ground state, so that one can expect a slight shortening of these bonds. Hence a movement of the phenyl groups might not even be necessary to achieve the geometrical rearrangement, and no viscosity effect is expected for the relaxation. The absence of a viscosity effect has been taken as evidence against a geometrical rearrangement involved in the decay X → Y, but only phenyl ring torsion and bending motions were considered in this context.[5]

We find that the fluorescence quantum yield approaches a limiting value of $\Phi_F^0 = 0.50$ at lowest temperature. Hence the decay chain proposed by HOMN (eq 1) must be modified to include a temperature-independent decay of 1^1B_{1u} bypassing the species 1^1A_u. Since the yield of triplets seems to be temperature independent, this decay must at least partly lead to the lowest triplet state 1^3B_{1u}. HOMN have in fact reported a component in the transient absorption of T with very fast (unresolved) rise time. The presence of this temperature-independent contribution to some extent explains the discrepancy between the values for the activation energy found by us (14 kJ/mol) and by HOMN (8 kJ/mol). Instead of $\ln \tilde{k}_X$, the difference $\ln(\tilde{k}_X - k_X^0)$ should be plotted against $1/T$, where k_X^0 is the decay constant of the fluorescing state in the limit of zero temperature. The data point at lowest temperature in ref 5 is $k_X = 10^9$ s^{-1} at $T = 120$ K. At this temperature the fluorescence quantum yield has almost reached its low-temperature limit, so that we may estimate $k_X^0 \approx 10^9$ s^{-1}. The Arrhenius analysis of the fluorescence decay rates from Figure 6 of ref 5 then yields an activation energy of $E_A \approx 11.5$ kJ/mol.

The INDO/S method also yields oscillator strengths for transitions between excited states. For the $S_1 \rightarrow S_n$ spectrum, two intense transitions are calculated at 11 993 cm^{-1} ($f = 0.210$) and 28 823 cm^{-1} ($f = 0.849$). Both transitions are polarized along the long molecular axis, i.e. lead to ^1A_g excited states. The calculated triplet–triplet absorption spectrum shows only one transition with an oscillator strength greater than 0.005, namely at 27 106 cm^{-1} ($f = 0.993$). This transition is also long-axis-polarized and leads to a state of A_g symmetry. To estimate the transient absorption of the species Y, which we assign to the 1^1A_u state, the calculation must be done near the equilibrium distance of this state at $R = 1.28$ Å. Only one transition with reasonable intensity ($f > 0.02$) is found, namely at 16 479 cm^{-1} ($f = 0.201$), leading to a state of B_{1g} symmetry. Compared to the transition frequencies observed for the three species in ref 5 (X, 20 000 cm^{-1}; Y, 14 300 cm^{-1}; T, 24 100 cm^{-1}), the calculated frequencies (28 823, 16 479, and 27 106 cm^{-1}) are somewhat too high.

Our model explains all observations made in the condensed phase for tolan. As the result of the crossing of the adiabatic potential energies of two electronic states, the lowest energy excited potential surface displays two minima. The first minimum is the

species X with $^1B_{1u}$ character. It is reached by vertical excitation from the ground state and is the initial state for the fluorescence of tolan. The second minimum with ^1A_u character is species Y. Since X decays to Y at room temperature without any detectable reverse reaction or establishment of equilibrium, Y must be lower in energy than X by at least 300 cm^{-1}. On the other hand, the non-Born–Oppenheimer coupling between both states is small, i.e. far from the statistical limit or even the intermediate coupling case, since the decay X → Y is suppressed at low temperatures. Hence the energy gap cannot be much larger than 1000 cm^{-1}. We prefer to view the decay X → Y as a photochemical reaction; i.e. X and Y could be regarded as excited-state isomers.

If one refers to the adiabatic potential curves, then 1^1B_{1u} is indeed the second excited singlet state since its minimum is higher than that of 1^1A_u. This is not, however, what HOMN had in mind when they assigned the fluorescence to the S_2 state, since they assumed a lower excited state at the same geometry. Such a situation seems very unlikely also in view of the fact that the fluorescence quantum yield approaches $\Phi_F = 0.50$ at low temperatures. This would be at least 1 order of magnitude larger than the largest quantum yield observed so far for a fluorescence from a higher excited singlet state of any polyatomic molecule.

Although reordering of the level structure through solvent effects is in principle possible, it may be asked whether the same picture applies also for the isolated molecule, in particular since the situation observed for tolan in the condensed phase is well represented by the calculation of the isolated molecule. Excitation spectra of tolan in a supersonic jet show weak lines to the red of the strong $1^1A_g \rightarrow 1^1B_{1u}$ transition. These lines could correspond to direct (nonvertical) excitation to the 1^1A_u state. For 2-(2′-hydroxyphenyl)benzothiazole, a molecule which undergoes intramolecular proton transfer in the excited state, direct nonvertical excitation of the tautomer was observed recently.[27] In this molecule the two wells of the S_1 potential surface are separated by only a small geometrical change, and the same seems to be true for tolan.

Conclusion

It is concluded that the optically allowed state 1^1B_{1u} is the lowest excited singlet state at the equilibrium geometry of the electronic ground state of tolan. This state is responsible for the entire fluorescence and the longest-wavelength absorption band of tolan. At larger distances of the central carbon atoms, another state, 1^1A_u, is lower in energy. In the isolated molecule nonvertical transitions to the 1^1A_u state could explain the weak lines to the red of the origin of the strong $1^1A_u \rightarrow 1^1B_{1u}$ transition. Although both states experience different solvent shifts, 1^1A_u is still the lowest excited state *at its own equilibrium geometry*. Hence the assignment of the fluorescing state to S_2 by HOMN is formally confirmed. The crossing from 1^1B_{1u} to 1^1A_u involves an energy barrier of 14.0 kJ/mol in the condensed phase. This decay has more similarity to an excited-state isomerization than to internal conversion. The failure to observe direct transitions to 1^1A_u in the condensed phase could be due to solvent effects on the equilibrium distance of the 1^1A_u state leading to very small Franck–Condon factors for transitions from the ground state.

Acknowledgment. This work was supported by the Fonds der Chemischen Industrie. C.F. gratefully acknowledges fellowships from the DAAD (Deutscher Akademischer Austauschdienst) and the Max Planck Society (through Prof. J. Troe). We also thank Dr. B. Nickel for valuable discussions, Dr. K.-H. Grellmann for the opportunity to use his fluorescence equipment, and the Gesellschaft für wissenschaftliche Datenverarbeitung Göttingen for providing computer time on the IBM 3090 mainframe.

References and Notes

(1) Okuyama, K.; Hasegawa, T.; Ito, M.; Mikami, N. *J. Phys. Chem.* **1984**, *88*, 1711.
(2) Gutmann, M.; Gudipati, M.; Schönzart, P.-F.; Hohlneicher, G. *J. Phys. Chem.* **1992**, *96*, 2433.
(3) Shacravorty, S. C.; Ganguly, S. C. *Z. Phys. Chem. (Munich)* **1970**, *72*, 34.
(4) Tanizaki, Y.; Inoue, H.; Hoshi, T.; Shiraishi, J. *Z. Phys. Chem. (Munich)* **1971**, *74*, 45.
(5) Hirata, Y.; Okada, T.; Mataga, N.; Nomoto, T. *J. Phys. Chem.* **1992**, *96*, 6559.
(6) Sidman, J. W.; McClure, M. S. *J. Chem. Phys.* **1956**, *24*, 757. Lacy, A. R.; Budy, R. G.; Frank, G.; Ross, I. G. *J. Chem. Phys.* **1967**, *47*, 2199.
(7) Huber, J. R.; Mahaney, M. *Chem. Phys. Lett.* **1975**, *30*, 410. Mahaney, M.; Huber, J. R. *Chem. Phys.* **1975**, *9*, 371.
(8) Plummer, B. F.; Al-Saigh, Z. *Y. Chem. Phys. Lett.* **1982**, *91*, 427.
(9) Henson, R. C.; Jones, J. L. W.; Owen, E. D. *J. Chem. Soc. A* **1967**, 116.
(10) Razumov, V. F.; Sazhnikov, V. A.; Alfimov, M. V.; Kotyarevskii, I. L.; Bardamova, M. I.; Vasilevskii, S. F. *Izv. Akad. Nauk SSSR, Ser. Khim. (Engl. Transl.)* **1979**, 329.
(11) Kühnle, W. *Woelm Inf.* **1970**, 5a.
(12) MOPAC version 4.00 vectorized for IBM3090: Stewart, J. J. P. *QCPE* **1987**, *4*, 560.
(13) Dewar, M. J. S.; Thiel, W. *J. Am. Chem. Soc.* **1977**, *99*, 4899.
(14) Dewar, M. J. S.; Zoebisch, E. G.; Healy, E. F.; Stewart, J. J. P. *J. Am. Chem. Soc.* **1985**, *107*, 3902.
(15) Del Bene, J.; Jaffé, H. H. *J. Chem. Phys.* **1968**, *48*, 1807, 4050; **1968**, *49*, 1221; **1969**, *50*, 1126.
(16) Dick, B.; Hohlneicher, G. *Theor. Chim. Acta (Berlin)* **1979**, *53*, 221.
(17) Dick, B.; Nickel, B. *Chem. Phys.* **1983**, *78*, 1.
(18) Dick, B.; Freund, H.-J. *Int. J. Quantum Chem.* **1983**, *24*, 747.
(19) Cohen, I. *J. Chem. Phys.* **1972**, *57*, 5076.
(20) Förster, Th. *Fluoreszenz Organischer Verbindungen*; Vandenhoeck und Ruprecht: Göttingen, Germany, 1951; p 158.
(21) Strickler, S. J.; Berg, R. A. *J. Chem. Phys.* **1962**, *37*, 814.
(22) Meech, S. R.; Phillips, D. *J. Photochem.* **1983**, *23*, 193.
(23) Elsaesser, T.; Lärmer, F.; Kaiser, W.; Dick, B.; Niemeyer, M.; Lüttke, W. *Chem. Phys.* **1988**, *126*, 405.
(24) Lin, H. B.; Topp, M. *Chem. Phys. Lett.* **1979**, *64*, 452.
(25) Hochstrasser, R. M.; Nyi, C. A. *J. Chem. Phys.* **1979**, *70*, 1112.
(26) Kellerer, B.; Hacker, H. H.; Brandmüller, J. *Indian J. Pure Appl. Phys.* **1971**, *9*, 903.
(27) Wiechmann, M.; Port, H. *J. Lumin.* **1991**, *48–49*, 217.
(28) Saebo, S.; Almlöf, J.; Boggs, J. E.; Stark, J. G. *J. Mol. Struct. (Theochem)* **1989**, *200*, 361.